Antenna Axis Offset and Intersection Determination using GPS

W. L. Combrinck

Hartebeesthoek Radio Astronomy Observatory, South Africa

C. L. Merry

Department of Surveying and Geodetic Engineering, University of Cape Town, South Africa

Abstract The determination of the axis intersection and offset of the HartRAO radio telescope and possible variation of these parameters due to gravitational distortion and temperature related expansion is described. Several algorithms for calculating these parameters are investigated and evaluated. Methods are developed to minimize the size and influence of errors. The results clearly show the feasibility of using GPS. This method has the added advantage of allowing the VLBI, SLR and GPS reference frames to be tied to a single point.

1 Introduction

Very Long Baseline Interferometry (VLBI) is a technique developed by astronomers to measure accurately the positions and spatial structure of astronomical radio sources utilising radio telescopes. VLBI has been used in an inverse way since the early 70's for high precision geodynamical studies by determining the position of and baseline between stations using observations of extragalactic sources (quasars). The Hartebeesthoek Radio Astronomy Observatory (HartRAO) currently supports several long term international geodetic VLBI projects.

The axis offset has been determined by VLBI and conventional surveying, but there is a difference of up to 17 mm between individual VLBI solutions and the Jet Propulsion Laboratory (JPL) standard value of 6706 mm. It is important to have an independent check of the HartRAO antenna axis offset in order to verify the results of the other techniques. This will increase the validity of the model for delay terms as used for the antenna and so improve the accuracy and reliability of geodynamical results which are derived from VLBI using the HartRAO antenna. This work will also allow the three reference systems; VLBI, Satellite Laser Ranging (SLR) and Global Positioning System (GPS) to be tied to a common point, i.e. the SLR reference marker.

The axis intersection (VLBI reference point) is, by definition, the intersection of the two axes, i.e. the Hour Angle (HA) and Declination (DEC) axis of a telescope. If these axes do not intersect as in HartRAO's case, it is the projection point of the secondary axis onto the primary axis. Before this point can be calculated the axis offset needs to be determined.

Depending on the mode of use and the GPS equipment used, high precision measurements can be made in geodetic applications. It is therefore utilised in geodetic programmes to supplement and strengthen the databases which are used to build models of the Earth's gravity fields, ocean tides, sea surface topography, orientation, global sea level and ocean circulation. It is very suitable for high precision short baseline work. GPS is seen as the primary tool of geodesists due to the dramatic improvements in techniques and software, availability and economical access to GPS equipment, portability and the benefits of international collaboration [*Blewitt*, 1993]).

Section 2 introduces the influence of the antenna axis offset on the VLBI delay model. Section 3 describes the methods, equipment and rationale used for sampling. Possible sources of error are described as well as preventative measures to reduce their magnitude. In section 4 the most successful approach to determine the antenna axis offset after data collection using GPS is presented. The suitability of other approaches are discussed. Analyses of the data and results found are described and discussed in the next section, followed by conclusions based on the results obtained. In this paper, the terms radio telescope and antenna are used to refer to the radio astronomy antenna, the term GPS antenna is specified when reference is made to the antenna used by the GPS receiver.

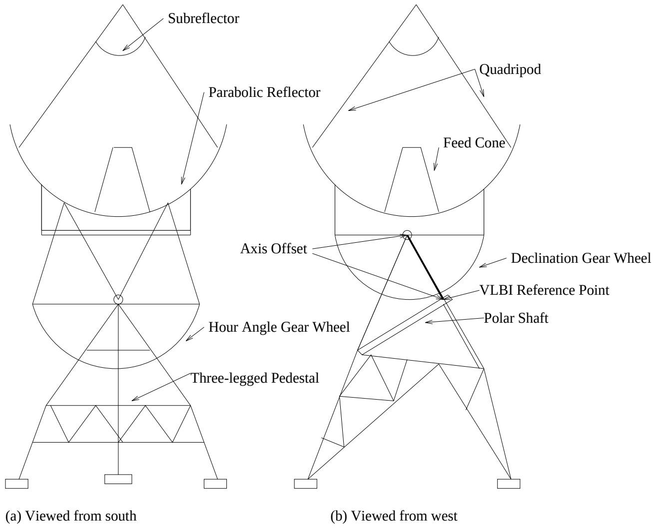

Figure 1: Simplified schematic of the HartRAO 26 m antenna illustrating the main structural components.

2 Axis Offset Influence on the VLBI Delay Model

The main components and configuration of the HartRAO radio telescope are depicted in figure 1. The antenna has an Hour Angle-Declination (equatorial) mounting, where the main axis (polar) is parallel to the Earth's rotation axis. In general, the travel time of a wavefront between the antennas at two or more sites is measured by maximizing the cross-correlation function of the different signals received at the antennas. The difference in travel time (group delay) is a function of the geometry of the participating stations, the spatial distribution of the radio sources, effects of the propagation medium and instrumental effects [*Kolaczek,* 1989]. The latter includes clock drifts and the offset of the antenna axes. The group delay is one of the parameters which allows solving for the baseline coordinates.

The observed values of delay and delay rate obtained from observations by a network of VLBI stations of a number of different radio sources have to be processed by software specifically developed for the task. This software contains a multiparameter estimation routine which solves for the model parameters. In general, the geometric component of the delay model is the most significant component with a delay as large as 20 ms with changes of up to $3.1\mu s$ per second as the Earth rotates.

2.1 Geometric Delay

A generalised antenna pointing system is shown in figure (2), with unit vector $\hat{s}$ pointing to the apparent source position. A symmetry axis AD is parallel to $\hat{\boldsymbol{s}}$. Point A is the end view of the DEC axis which rotates in the plane perpendicular to the axis. A distance H, which is the antenna axis offset, separates the DEC

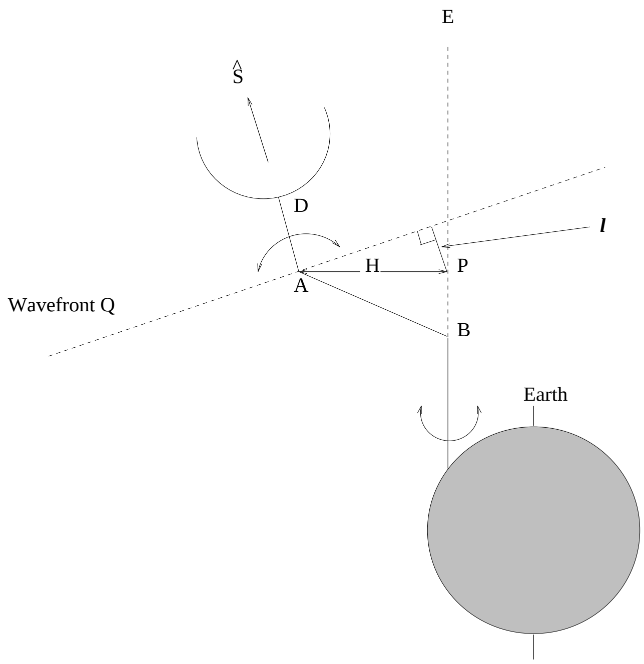

Figure 2: Generalized schematic representation of the geometry of a two-station VLBI network. Only one station is shown. Adapted from *Sovers and Jacobs* [1994].

axis from the second rotation axis which is the polar axis BE. Point P, the VLBI reference point, is the intersection of the HA and DEC axes of a telescope. If these axes do not intersect as in HartRAO's case, it is the intersection point obtained when the plane containing the secondary axis A and perpendicular to BE is projected onto the primary axis BE.

The plane Q, which contains the rotation axis A, is an isophase plane for plane wave fronts as it coincides with the wave front. If l is the length of a line from P to the Q plane and is perpendicular to that plane, the wave front will reach the axis intersection point P at a time $\Delta = l/c$ after the wave passes through axis A. If τ_0 is the model delay for a wave front to pass from P on antenna N^o 1 to a point P on antenna N^o 2, the model should be changed to:

$$\tau = \tau_0 - (\Delta t_2 - \Delta t_1) = \tau_0 + (l_1 - l_2)/c. \quad (1)$$

The subscripts refer to antennas N^o 1 and N^o 2. Following a treatment by *Sovers and Jacobs* [1994] two other coplanar vectors, a unit vector $\hat{\boldsymbol{I}}$ along BE and positive away from Earth, and $\boldsymbol{L}$ from P to A are defined. Then one has

$$\boldsymbol{L} = \pm H \times \frac{\hat{\boldsymbol{I}} \times [\hat{\boldsymbol{s}} \times \hat{\boldsymbol{I}}]}{|\, \hat{\boldsymbol{I}} \times [\hat{\boldsymbol{s}} \times \hat{\boldsymbol{I}}]\, |} \quad (2)$$

Where the $\pm$ is chosen to give $\boldsymbol{L}$ the direction from P to A. Since

$$\hat{\boldsymbol{I}} \times [\hat{\boldsymbol{s}} \times \hat{\boldsymbol{I}}] = \hat{\boldsymbol{s}} - \hat{\boldsymbol{I}}[\hat{\boldsymbol{I}} \cdot \hat{\boldsymbol{s}}] \quad (3)$$

then

$$l = \hat{\boldsymbol{s}} \cdot \boldsymbol{L} = \pm H \sqrt{1 - [\hat{\boldsymbol{s}} \cdot \hat{\boldsymbol{I}}]^2} \quad (4)$$

The antenna axis offset therefore has a direct impact on the accuracy of the delay model by affecting the value of l.

Antenna Axis Offset Altitude Correction: The secondary rotation axis of Equatorial mounts has a vertical movement with changing dish orientation. This is the DEC axis A in Figure 2. This vertical movement leads to variation in the zenith troposphere delay of 1 - 2 mm. This zenith variation is increased by the mapping function to 1 - 2 cm when the antenna is pointing towards a source at low elevation. The correction added to the zenith dry tropospheric delay in the model used by *Sovers and Jacobs* [1994] is

$$\delta_\tau = -\rho z_{dry}(\frac{H}{\Delta})\psi. \quad (5)$$

Here ρz is the additional delay at local zenith due to the troposphere, H is the antenna axis offset, ψ is an angular factor which depends on the type of antenna mounting and Δ is the dry troposphere scale height ($\sim$ 8.6 km). For the HartRAO antenna,

$$\psi = \cos\phi \cos h, \quad (6)$$

where h is the local Hour Angle east of the meridian and ϕ is the geodetic latitude.

3 Experimental Method and Data Collection

The basic network consisted of three GPS receivers. A GPS antenna was mounted on the vertex of the quadripod. A stationary GPS receiver was located on the SLR reference pier and a 3rd receiver was stationed on the cement roof of the main building for which a brass stud served as reference. The distance from the receivers on the roof and SLR pad to the telescope was approximately 60 m. The telescope was moved on its axes, allowing the GPS antenna to trace an arc in space. Points were sampled on two arcs, the DEC arc which is traced when the HA axis is fixed and the HA arc when the DEC axis is fixed. The vectors of the GPS receivers to the telescope intersected approximately at right angles. The receiver on the roof was only used as a control as it was inferior to the data collected on the SLR pad.

3.1 GPS Antenna Gimbal

Moving the telescope away from the zenith point in either axis would cause a tilt of the GPS antenna away from its horizontal position. This would cause a shift of the antenna phase centre. To prevent this, a gimbal was designed to support the GPS antenna at the apex of the quadripod of the telescope. The axes of the gimbal intersect at right angles and the point of intersection was designed to coincide with the antenna phase centre.

Table 1: Data set 1: GPS050; Zenith point statistics.

Coordinate	Value (m)	σ (mm)	Δ (mm)
$\overline{X}$	60.1094	2.5	0.6
$\overline{Y}$	-56.9381	1.9	0.4
$\overline{Z}$	-15.0078	2.3	0.5

3.2 Data Sets

The first data set was sampled randomly so as to alleviate any systematic errors, thus there was no fixed sequence as to the points visited.

GPS048 and GPS052 There are two arcs which the GPS antenna describes when the telescope is moved in either axis with the other axis fixed. First, an arc on a great circle when the DEC axis is moved with fixed HA axis. Second, an arc on a small circle when the DEC axis is fixed and the HA axis is moved. The *zenith point* of the telescope is the point where the dish is horizontal and is facing straight up. Points were measured on the DEC arc with a spacing of 8° and on the HA arc with a spacing of 32′ as this gave reasonable arc lengths and point distribution for the available telescope time.

GPS050 During this session the telescope was kept stationary at zenith. It was hoped that this would allow the thermal signature of the telescope to be found. Unfortunately the temperature differential was small during the duration of the session. Thermal transducers positioned on the three legs and close to the HA encoder allowed thermal monitoring. The mean values and statistics are listed in table 1. Considering the fact that 1-3 mm vertical movement could be due to thermal expansion, the standard deviations and standard errors are very acceptable and indicate no multipathing.

3.3 Data Set 2: GPS213; GPS215

As a result of experience gained during attempts at determining the offset from data set 1, the following ideas were incorporated into data set 2:

(1) A stand-alone thermal model was not feasible unless a very large number of points could be measured for many days. It was therefore decided to sequence the visits to individual points in such a way that a thermal model would be implicit in the solution of the circle centres. This was done by including a zenith point visit at every 3rd point to be measured. The observing sequence followed a fixed pattern, so that any given set of three points, such as 1, 2, 3 or 25, 26, 27 could be used by the centre finding software to determine the circle centre. As the temperature changed, the combination of the three points were always temperature related within the three hours, with the zenith as mid-observation. In sessions GPS048 and GPS052, temperature differentials as large as 20° C occurred between points as a result of the random sequence of point visiting.

(2) Measuring evenly distributed points on arcs of about $\sim 90°$ were not the optimum type of distribution for solving the circle centres. Combinations of points close to the zenith point led to larger errors due to smaller angular separation. There is a restriction of $\sim 45°$ of the arc on either side of the zenith point due to GPS signal spillover from the telescope dish to the GPS antenna, so that the arc lengths could not be increased significantly. Consequently, two smaller, more dense arcs were measured on the outer edges of the arcs. This meant that for every individual solution, adequate angular separation was provided for.

3.4 GPS Error Sources

In general the vertical component has a greater standard deviation than the horizontal components. This is due to the fact that the vertical component is not as constrained and is more sensitive to errors in tropospheric delay [*Blewitt*, 1993]. Precision in the vertical component increases with a larger number of satellites being observed simultaneously as the correlation coefficient between the vertical station coordinate and zenith tropospherical delay decreases.

The unpredictable behaviour of the time and frequency standards serving as a reference for GPS receivers is the main source of error in a measurement. By the process of differencing, the errors resulting from receiver and satellite clocks can be virtually eliminated. Differencing can be done between receivers, satellites, epochs or a combination of these. Expressions for the various differencing techniques can be found in *Leick* [1990]. Differencing reduces the effect of the ionosphere and troposphere when receivers are close to each other, so that dual-frequency operation is not necessary for short ($\sim$ 3 km) baselines. With the double difference observable the effect of instabilities in the receiver and satellite oscillators are largely cancelled. This observable was used to determine the data points in this work.

3.4.1 GPS Antenna Phase Centre

The antenna electrical phase centre is the reference point to which the radio signal measurement is made. This phase centre does not correspond exactly to the physical antenna centre and this offset is dependent on the elevation, azimuth and intensity of the satellite signal. Two effects should therefore be taken into account, namely the antenna phase centre variation and the offset. The antenna phase centre is not located at the same point for widely varying incident signal elevation angles, which adds to the total error in the positional computation. The gimbal's axis of rotation was set up to intersect the phase centre, so that movement of the telescope from data point to data point would have as little effect on the phase centre as possible.

3.4.2 Multipathing

A problem which gives rise to even larger errors than phase centre variations when using a conventional wide beamwidth GPS antenna is multipathing. This occurs when the satellite signal arrives at the antenna via different paths, after reflection of the incident wave by a reflecting surface. The received signals will show relative phase offsets due to different path lengths. There are several ways in which the multipathing for normal GPS surveying applications can be reduced, but if a normal wide beamwidth GPS antenna is mounted in a conventional way on the main dish, the parabolic shape of the dish and large reflective area of the cone could cause serious multipathing. It was initially thought that several centimetres of error would be present in the baselines due to multipathing. Furthermore, the main dish is located in a valley where reflection off the slopes of the surrounding hills could add to the problem. The environment in which the measurements were to take place could require that techniques be adopted to detect the presence of multipathing. This is especially true if the elevation of the dish was such that spillover from the dish to the GPS antenna could take place.

A large reflective backplane should reduce spillover from the dish surface to the GPS antenna and as the GPS antenna has a large backplane, it was relied upon to reduce spillover. The duration of the visits to a specific point during the sessions was one hour, as this was thought to be adequate to negate the effects of possible multipathing due to change in satellite geometry over the duration of the session. In order to find possible signs of multipathing, several of the sessions were broken up into six smaller ten minute segments and reprocessed. The repeatability of the solutions of individual ten minute sessions were within 3-4 mm, which indicated that little or no multipathing was present. Deviations of some centimetres would be expected if multipathing was present. The one hour duration of the sessions, as well as making sure that the elevation angle of the telescope was kept to the limit where no spillover from the dish could be picked up by the GPS antenna, seemed to be adequate in preventing serious multipathing.

3.4.3 Accessibility to GPS Signals

There is a considerable amount of shadowing due to the size and proximity of the main dish to the GPS antenna. The effective horizon of the GPS antenna will change with the elevation of the main dish, therefore at elevations $< 45°$ the satellite availability will be adversely affected. The telescope was never steered to elevations $< 45°$ to avoid this problem.

3.4.4 Solution Error Sources

With carrier phase measurements, the aim of data processing is to resolve the initial double difference phase ambiguities of the carrier phase [*Nolan et al.*, 1993]. After determination of the ambiguities, millimetre position results are possible. The signals from the receivers are compared by a process of subtraction, and the relative position of the GPS antenna on the main dish to the GPS antenna on the SLR reference pier and main building roof is then determined by the difference signals. This differential positioning is required to remove errors common to all the receivers, such as satellite clock and ephemeris errors, selective availability as well as unmodelled ionospheric and tropospheric propagation errors. The removal of errors is due to the fact that corresponding signals from the two receivers are subtracted, so errors which are common to both receivers are cancelled out to a large degree as described in the next paragraphs.

Selective Availibility Errors Intentional dithering of the satellite frequencies, which introduce errors in the navigation time coded signals as well as intentional changes to the ephemeris parameters were compensated for by using double differencing during the processing stage.

Ionospheric Delay Errors The signal propagation delay can change by up to 6 m at night and 30 m by day. For short baselines as in this case, the ionospheric delay is basically the same for all receivers. This is primarily due to the fact that the signal path from a given satellite as seen from the receivers is essentially the same.

Tropospheric Delay Errors This effect has a magnitude of up to 3 m and is maximum for satellites at low elevation. The extent of this effect was reduced by using a horizon mask of 15° to exclude satellites at a low elevation. The same reasoning for ionospheric delays are applicable, so that compensation is almost total for short base lines.

Ephemeris and Clock Errors Clock errors are compensated for by the double difference solution as explained in section (3.4) when the receivers in the network employ the same satellite data.

4 Offset Determination Methods

Three separate approaches were used to determine the centres of the DEC and the HA circles; analytical geometry, which included the intersection of two co-planar lines and the intersection of three planes; intersection of three planes using matrices; and circle function fitting using least-squares. The offset could be found once these circle centres had been determined. An application of analytical geometry (intersection of co-planar lines) was developed which is more robust and accurate on this type of data distribution than the other methods and is described in some detail. The other intersection methods are not described.

4.1 Least-Squares

Least-squares was found to be unsuitable to determine the DEC and HA circle centres. It did however find application in modelling the spherical function, using the centre coordinates and radius found with the method described in section 4.2. This allowed parameters for gravitational distortion to be modelled in the spherical function. This is discussed in greater detail in section 4.5.4.

In this work, an adaptive nonlinear least-squares algorithm was used as developed by *Dennis et al.* [1981]. The algorithm maintains a secant approximation S to the second-order part of the least-squares Gauss-Newton Hessian and adaptively decides when this approximation is to be used.

During attempts to use least-squares to fit the function of a sphere to the data, an acceptable fit could not be found. Even constraining several or all of the parameters produced poor results. Several problems arise when using least-squares to fit a circle or a space curve to data. The problems experienced are directly related to the criterion used for minimization; several of these problems are described in *Chan* [1965]; *Kása* [1976]; *Angel and Barber* [1977]; *Anderson* [1981]; *Berman and Culpin* [1986]; *Gates* [1993] and *Gates* [1994].

It is generally apparent that for data on an arc which is less than a semicircle, estimation by least-squares is unsatisfactory. Convergence is made difficult as the error range is of the same order of magnitude for a large range of radii. *Angel and Barber* [1977] predict that any estimation method will experience difficulties for data where $T < [0, \pi]$. T is the polar angle in radians. Least-squares estimators and maximum likelihood estimators both fail to be consistent methods, especially when the distribution of the points on the circle is not over the total circumference.

4.2 Intersection of Co-Planar Lines

The most successful method to find the circle centres and axis offset used the point of closest intersection of two co-planar lines. Consider three measured points on the DEC curve, (P_1, P_2, P_3) as depicted in figure 3. In figure 3 $d_1 = P_1P_2$, $d_2 = P_2P_3$, $d_3 = P_3P_1$, $d_4 = P_1P_6$, $d_5 = P_3P_8$, $d_6 = P_4P_9$ and $d_7 = P_5P_9$. The circle centre is P_9. The DEC curve is the space curve traced by the GPS antenna as it was moved in declination. This discussion is also valid for data points on the HA curve. Analytical geometry is used to derive the centre and the radius. Only three points on a circle are required to define the circle [*Briggs and Bryan*, 1910] and one can use the perpendicular bisector of the chords P_1P_2 and P_2P_3 to determine the circle centre. Using direction cosines and the equation for an angle between two lines, one can find the expressions for $\cos\theta$ and $\cos\gamma$. The length of lines d_1, d_2 and d_3 are found from the equation of the true length of a space line and the line lengths d_4 and d_5 would then be

$$d_4 = \frac{(d_1 \times 0.5)}{\cos\theta} \tag{7}$$

and

$$d_5 = \frac{(d_2 \times 0.5)}{\cos\gamma}. \tag{8}$$

The perpendicular bisector of chord d_1 then intersects chord d_3 in P_6 and the perpendicular bisector of chord d_2 intersects chord d_3 in P_8. The points P_4 and P_5 are found by using an equation for the mid-point of a line.

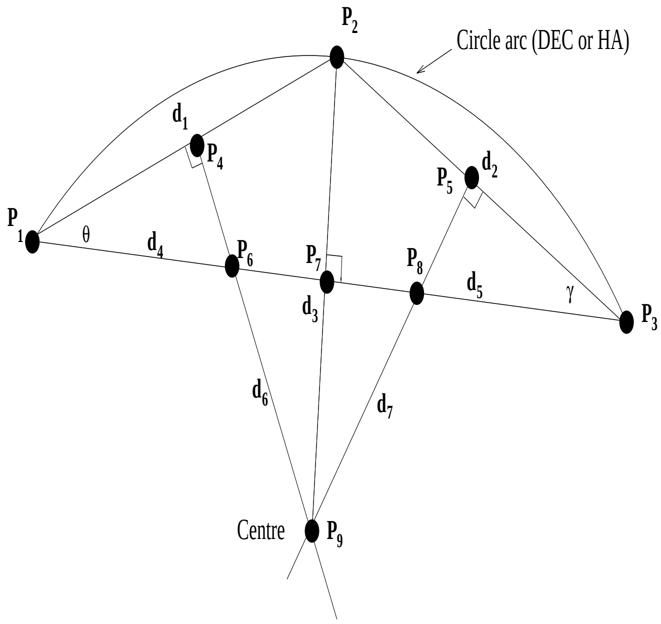

Figure 3: Centre of circle found by spatial intersection.

Using proportions, the coordinates of P_6 and P_8 are

$$x_6 = x_1 + \frac{d_4}{d_3} \times (x_3 - x_1) \tag{9}$$

$$y_6 = y_1 + \frac{d_4}{d_3} \times (y_3 - y_1) \tag{10}$$

$$z_6 = z_1 + \frac{d_4}{d_3} \times (z_3 - z_1) \tag{11}$$

and

$$x_8 = x_3 + \frac{d_5}{d_3} \times (x_1 - x_3) \tag{12}$$

$$y_8 = y_3 + \frac{d_5}{d_3} \times (y_1 - y_3) \tag{13}$$

$$z_8 = z_3 + \frac{d_5}{d_3} \times (z_1 - z_3) \tag{14}$$

The intersection of the two co-planar lines utilises the parametric representation of a line which is rearranged to enable extension of the line by using the fact that the two points P_4 and P_6 define the inclination of the line d_6 using their direction ratios. Similarly the two points P_5 and P_8 define the inclination of the line d_7. One can therefore use the equations

$$\left.\begin{array}{rcl} x_{d_6} & = & (x_6 - x_4) \times kv + x_4 \\ y_{d_6} & = & (y_6 - y_4) \times kv + y_4 \\ z_{d_6} & = & (z_6 - z_4) \times kv + z_4 \end{array}\right\} 0 \leq kv \tag{15}$$

and

$$\left.\begin{array}{rcl} x_{d_7} & = & (x_8 - x_5) \times kv + x_5 \\ y_{d_7} & = & (y_8 - y_5) \times kv + y_5 \\ z_{d_7} & = & (z_8 - z_5) \times kv + z_5 \end{array}\right\} 0 \leq kv \tag{16}$$

to calculate the intersection of lines d_6 and d_7. The radius is calculated by finding the distance between the intersection P_9 and point P_2. The value of kv is then incremented by a subroutine which makes use of the straight line distance between the calculated points on lines d_6 and d_7 as determined from equations (15) and (16). The closer the intersection becomes, the smaller the incremental addition to kv. The convergence is stopped when the separation between the lines reaches either 5×10^{-9} metres or divergence is detected.

A figure of merit is generated for each centre solution, which is basically a modified least-squares error criterion,

$$FM = (R_i^2 - \overline{R}^2)^2 \tag{17}$$

The figure of merit is sensitive to deviations from the mean and was found very useful in evaluating individual intersections.

Figure 4 depicts the DEC and HA circles where the plane of the HA circle is normal to the plane of the paper, the curve of the DEC axis is an arc of a great circle. The telescope zenith point is P_1, P_2 is the DEC shaft seen end on, P_3 is the centre of the HA small circle, P_4 is the normal projection from P_2 onto P_1P_3, the common intersection of P_4P_6 and P_2P_3 is P_5 and P_6 is the VLBI reference point. The curve of the HA axis is a small circle, the centre of which is not the centre of the sphere which would be intersected by the polar shaft.

The equation

$$H = R_{HA} - R_{DEC} \times \cos\alpha \tag{18}$$

gives the offset solution for a given HA circle radius R_{HA} and DEC circle radius R_{DEC}. The cosine of the angle α is calculated using the equation for the true angle between two intersecting lines. The offset H can also be found by calculating the lines P_1P_2, P_2P_3 and P_3P_1 by following a similar approach as described in section 4.2. This is in fact done in the software as an additional check on the offset values. The coordinates of the VLBI reference point P_6 are determined by first calculating P_4 using proportions, where

$$x_4 = x_1 + \frac{d_1 \cos\alpha}{d_3} \times (x_3 - x_1), \tag{19}$$

$$y_4 = y_1 + \frac{d_1 \cos\alpha}{d_3} \times (y_3 - y_1), \tag{20}$$

$$z_4 = z_1 + \frac{d_1 \cos\alpha}{d_3} \times (z_3 - z_1). \tag{21}$$

Then the midpoint between P_2 and P_3 is determined which allows the VLBI reference point to be calculated using direction ratios. The offset is calculated as the distance from P_2 to $P6$ and from P_4 to P_3 as a check.

4.3 Errors

4.3.1 DEC and HA Circle Errors

The measured points on the DEC and HA circles x_i, y_i, z_i where $i = 1, \ldots, N$ are given by

$$\left.\begin{aligned} x_i &= x_{i0} + \varepsilon_i, \\ y_i &= y_{i0} + \zeta_i, \\ z_i &= z_{i0} + \eta_i. \end{aligned}\right\} \tag{22}$$

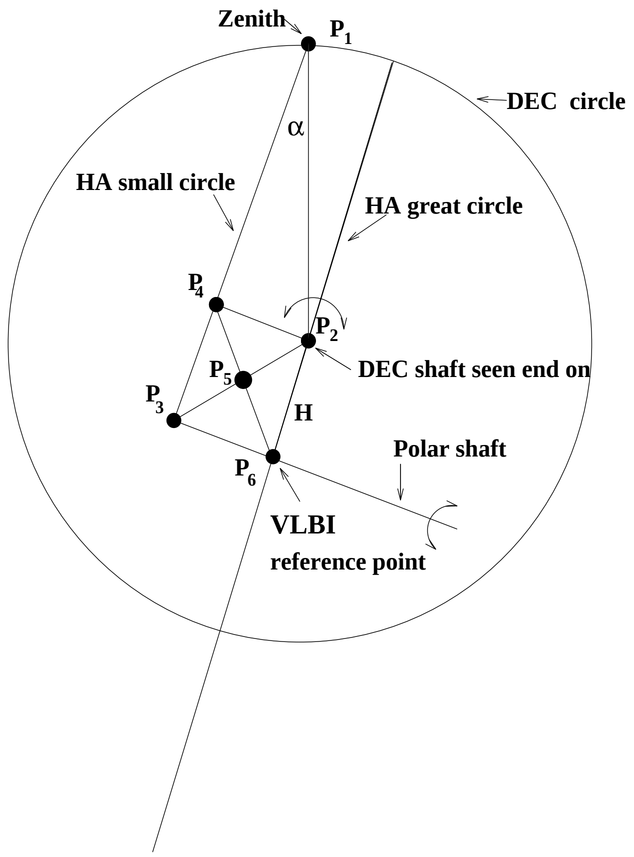

Figure 4: Dec and HA circle planar representation.

where $(\varepsilon_i, \zeta_i, \eta_i)$ is an error component consisting of several independent errors. Amongst these errors are ΔT, an error resulting from contraction and expansion of the antenna metal structure, and ΔP, an error resulting from the inability of the antenna to return to an exact point specified, i.e. a pointing error. Added to these error components is ΔU, a combination of many errors, which includes errors of the GPS observables such as tropospheric and ionospheric effects, multipathing, as well as antenna phase centre variation. It also includes the possible movement of the gimballed GPS antenna caused by high winds and perching birds. The error due to the gimbal swinging should be very small, as both rotation axes intersected the centre of the GPS antenna which is close to the phase centre. Errors due to wind loading on the antenna structure and gravitational loading are also contained within ΔU. Including these errors one can write equation (22) as

$$\left.\begin{aligned} x_i &= x_{i0} + x\Delta T_i + x\Delta P_i + x\Delta U_i, \\ y_i &= y_{i0} + y\Delta T_i + y\Delta P_i + y\Delta U_i, \\ z_i &= z_{i0} + z\Delta T_i + z\Delta P_i + z\Delta U_i. \end{aligned}\right\} \tag{23}$$

The errors may be dependent or independent. For instance the error ΔP resulting from driving the antenna in HA is largely dependent on the position from which the antenna is driving and the distance which it is driven. It is only dependent in the HA drive, the DEC drive seems to be independent. The error ΔP will also have a smaller random component due to peculiarities of the gears, drive, etc.

All the other sources of error such as ambient temperature variation, wind loading, troposphere and ionosphere are regarded as being mostly random. The error ΔT was minimized by observing points in a thermal sequence as discussed in section 3.3 and is discussed in more detail in section 4.5.3. The pointing error ΔP was reduced by a process of averaging and translation as described in section 4.4.1. The remaining error component, ΔU, was minimized by double difference processing, gimballing the antenna and one hour long visits to a specific station. An attempt to model some gravitational deformation using least-squares (see section 4.5.4) was made to ascertain the magnitude of this component.

4.4 Offset Determined from Data Set 2

4.4.1 Zenith Position

The zenith point is the only point which is common to both DEC and HA circles. This point is crucial for the determination of the offset as explained in section 4.2. The pointing error ΔP only influences the determination of the zenith point, as it is assumed to be a fixed point to which the antenna is returned to. On any other points of the HA and DEC circles, the antenna pointing is of less consequence, as we are then only interested in the GPS measured position.

Plots (see figure 5) of the uncorrected HA circle zenith points clearly shows a separation of the measured points into two groups, with maximum extension in the y coordinate. This grouping is due to hysteresis in the movement of the antenna. When the antenna drives from west to east the y coordinate is less than it should be. The antenna slightly overshoots and then moves back a bit more than the initial overshoot. The converse is true when driving from east to west and the y coordinate is more than it should be.

Pointing error correction The coordinates of the zenith were found by correcting for pointing error by a process of averaging and translation. The arithmetic average of groups 1 and 2 were found, which allowed one to find the centre of the line connecting the two average points. Groups 1 and 2 were then corrected with the value of the differential between the centre of the line and the average value of each group. The effect of the pointing error correction is shown in figure 5. The uncorrected Y coordinate in graphs (a) and (c) shows a spread around the average of more than ± 4 mm. After pointing corrections, the spread decreased to less than ± 3 mm and the grouping of the y coordinates was much more centred. Table 2 contains the average of the group coordinates. The coordinates (X_c, Y_c, Z_c) are the coordinates of the centre of the line connecting groups 1 and 2. After this pointing correction, the standard deviation (σ) and standard deviation of the mean (Δ) of the offset value were reduced from 19.6 mm to 18.4 mm and from ±3.1 mm to ±2.7mm respectively.

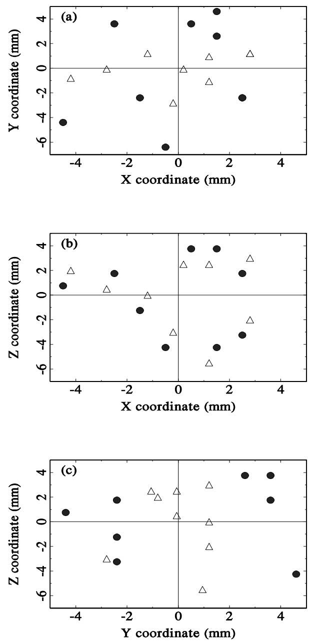

Figure 5: Graphs of coordinates, both corrected and uncorrected for pointing errors are shown. The triangles denote corrected coordinate and the filled circles the uncorrected coordinate. (a) Y vs X. (b) Z vs X. (c) Z vs Y. Coordinates have been normalised to the mean value.

Table 2: Summary of zenith group coordinates means and statistics: GPS213.

Group	Coordinate	Mean (m)	σ (mm)	Δ (mm)
0	X_c	60.1555	4.6	1.5
0	Y_c	-56.8896	2.7	0.9
0	Z_c	-15.0108	5.2	1.7
1	$\overline{X}$	60.15520	2.9	1.3
1	$\overline{Y}$	-56.8932	1.8	0.8
1	$\overline{Z}$	-15.0120	2.5	1.1
2	$\overline{X}$	60.1558	1.9	0.9
2	$\overline{Y}$	-56.8860	0.9	0.4
2	$\overline{Z}$	-15.0095	3.8	1.9

Adjusting centre coordinates A further adjustment is necessary. The DEC circle has defined a zenith point which required no pointing correction and the HA circle defined a zenith point after pointing correction. There is a small difference between these two zenith points as they are independent determinations. The offset calculation however requires that the zenith point be common to both circles. This meant that the circle centre values had to be translated with the differential between the average of the two zenith points and the individual zenith points, a similar process as used for the pointing

Table 3: VLBI reference point: Data set 2.

Coordinate	Value (m)	σ (mm)	Δ (mm)
x	41.680	15.8	2.0
y	-66.564	7.5	0.5
z	-8.131	3.9	0.1

correction. The adjustment values found were small, 0.185 mm, 1.150 mm and -1.025 mm. This brought a further reduction in the standard deviation and standard deviation of the error of the offset value, i.e. to 16.7 mm and to $\pm$2.3 mm respectively.

4.5 HA and DEC Circle Centre Determinations

4.5.1 Offset Determinations

The best estimate is 6.6956 $\pm$ 0.0023 m with a standard deviation of 16.7 mm. The errors are from independent solutions using independent points. There were ten and thirteen individual circle centre solutions for the HA and DEC circles respectively.

4.5.2 VLBI Reference Point

The VLBI reference point is the intersection of the two axes as described in section 4.2 and in this work is referenced to the SLR reference point. The final results obtained are listed in Table 3. This determination using GPS allows the three reference frames, GPS, SLR and VLBI, to be tied to a single point. This is possible due to the visit to the SLR site by a mobile satellite ranger of the Institute für Angewandte Geodasie (IfAG) during 1993, together with their occupation of the SLR reference point with a GPS receiver during their February 1995 Antarctica campaign.

4.5.3 Thermal Modelling

Tests were run to see what the effect on the offset value would be if instead of the implicit thermal model, random solutions were used. A typical result shows an offset value of 6.6951 m with a standard deviation of 19.7 mm and standard error of the mean of $\pm$3.1 mm. These values are both poorer than when the implicit thermal model is used.

4.5.4 Gravitational Effects

Least-squares was used to determine fits of circles and ellipses with and without sine gravity terms. As previously discussed, least-squares is not a feasible method to determine circle parameters when using less than a semi-circle. Consequently, the circle centre for the HA circle was used as a pivot point to rotate the HA arcs and zenith data through 180 degrees to create an image of the data in the same plane. This was done by using vector products to find a vector of rotation normal to

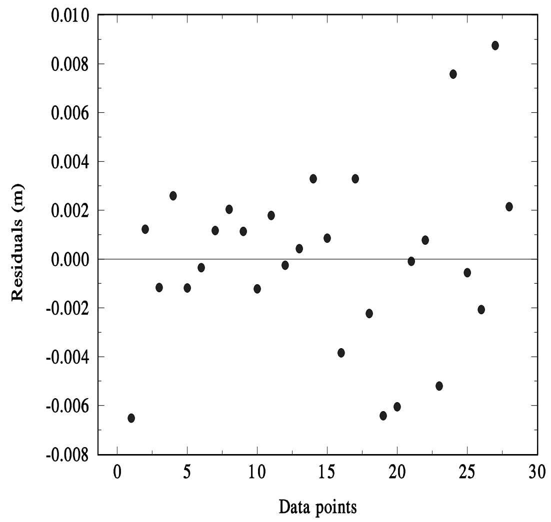

Figure 6: Residuals of HA circle least-squares fit as a function of data points.

the plane and through the circle centre. Although these data did not allow a unique circle centre determination, it did provide some information on the residuals between a theoretical circle and the data using the circle centre coordinates determined using the method described in section 4.2. The residuals as a function of data points are plotted in figure 6. Maximum deviation was 8.8 mm with an average deviation of 2.6 mm. Standard error of the estimate was 3.9 mm.

Fitting an ellipse showed conclusively that the circle data in fact describes a circle as the a (major axis) and b (semi-major axis) parameters of the ellipse differed by only 0.5 mm. It was thought that using the HA circle data would indicate some structural sagging or deformation as the HA axis carries the larger weight of the two and is subjected to the most leverage. If some bending took place a sine term would result, and the radius value should decrease. Adding sine gravity parameters to the circle and ellipse functions produced parameter values on the order of 10^{-7}. No conclusive evidence of gravitational deformation was found.

4.6 Comparison of Results from Different Methods

In the summary below the first two VLBI solutions by Marshall Eubanks (USNO) (personal communication) and Chopo Ma (NASA/GSFC) (personal communication) were found by adjusting HartRAO as well as the other fixed stations, in a VLBI solution along with geodetic, astrometric, station clock and atmosphere parameters. The solution by Mark Newling (Surveys and

Land Information) (personal communication) was found using conventional surveying methods. The last VLBI (1996) estimation by Chopo Ma shows a significant reduction in the size of the offset. The main difference between this and the 1995 solution is the estimation of atmosphere gradients. The gradients seem to improve geodetic consistency and are reasonable in terms of global atmospheric distribution.

(1) Standard Value (JPL Progress Report 42-49) 6706 mm

(2) Conventional surveying 1993: Mark Newling 6695 $\pm$ 3mm

(3) VLBI 1995: Chopo Ma 6693.6 $\pm$ 2.5mm

(4) VLBI 1995: Marshall Eubanks 6692.5 $\pm$ 1.5 mm

(5) HartRAO GPS solution 1995: 6695.6 $\pm$ 2.3 mm

(6) VLBI 1996: Chopo Ma 6688.8 $\pm$ 1.8 mm

With the exception of the standard value and Chopo Ma's 1996 estimation, all other solutions are within the errors of the GPS solution. Using GPS, the data required for a solution can be sampled in three days.

5 Conclusions

In order to realise millimetre precision in geodetic VLBI, parameters such as the axis offset must be known to a high degree of accuracy. It has a direct impact on the VLBI delay model by influencing the dry tropospheric and geometric delay. GPS can be used as a fast and efficient method to determine the axis offset and VLBI reference point. In order to use the GPS data however, the proper method for the determination of the circle centres and other parameters must be used. The applicability of GPS when used in close proximity to a large metal structure, even one that has been especially designed to reflect radio waves, has been demonstrated.

Of the three approaches to find circle centres as discussed, the circle centre finding algorithm which proved to be the most suitable for this work was the spatial intersection of two co-planar lines as described in section 4.2. The data sampling and experimental method could be optimized for this method. This method requires only three data points for a single solution and is very robust. It is clear that least-squares is not a suitable method for determining the circle centre of data describing less than a semi-circle, but it can be used once the centre has been determined to calculate the residuals between a theoretical circle and the GPS data and for modelling functions.

This work demonstrates an independent, efficient method of determining the antenna axis offset and VLBI reference point. These values compare very well with those found using other techniques.

This method does however have the distinct advantage that as in our case, having an SLR reference point available, which has been visited by both GPS and SLR, the three reference frames, VLBI, SLR and GPS can be tied to the same point.

Acknowledgements. We thank the following persons; the director of HartRAO, George Nicolson for continued support, Gerhard Soltau (IfAG) and Keith Greggor (University of Pretoria) for the use of their GPS receivers, Gordon McLeod, Derck Smits and Peter Stocker for thorough and constructive reviews of the manuscript.

References

Anderson, D.A. The Circular Structural Model. *J.R. Statist. Soc. B, 43, 2*, 131-141, 1981.

Angel, I. and Barber, J. An Algorithm for Fitting Circles and Ellipses to Megalithic Stone Rings. *Science and Archaelogy, 20*, 11-16, 1977.

Berman, M. and Culpin, D. The Statistical Behaviour of Some Least Squares Estimators of the Centre and Radius of a Circle. *J.R. Statist. Soc. B. 48, 2*, 183-196, 1986.

Blewitt, G. Advances in Global Positioning System technology for Geodynamics Investigation: 1978-1992, in *Contributions of Space Geodesy to Geodynamics.* eds. Smith, D.E and Turcotte, D. L. Geodynamics Series. Vol.25, 1993. American Geophysical Union. Washington, D.C. USA.

Briggs, W and Bryan, G.H. *The Right Line & Circle (Coordinate Geometry).* 3rd edition. University Tutorial Press, London, 1910.

Chan, N.G. On Circular Functional Relationships. *J.R. Statist.Soc.B, 27,* 45-46, 1965.

Dennis, J.E, Gay, D.M and Welsch, R.E. Algorithm 573 NL2SOL - An Adaptive Nonlinear Least-Squares Algorithm [E4]. *ACM Transactions on Mathematical Software, 7, 3*, 369-383, 1981.

Gates, J. Testing for Circularity of Spatially Located Objects. *J. Appl.Stat., 20, 1,* 95-103, 1993.

Gates, J. Distance Mean and Variance Functions and Sphere Fitting. *Statistics, 25*, 251-266, 1994.

Kàsa, I. A Circle Fitting Procedure and its Error Analysis. *IEEE Trans. Instrumentation and Measurement, 25*, 8-14, 1976.

Kolaczek, B. Earth Rotation Monitoring, in *Reference Frames in Astronomy and Geophysics.* (eds. Kovalesky, J., Mueller, I.I and Kolaczek, B.) Kluwer Academic Publishers, London, 1989.

Leick, A. *GPS Satellite Surveying.* John Wiley & Sons, New York, USA, 1990.

Nolan, J.M., Webster, I.R., Gourevitch, S.A. and Ladd, J.W. Rapid Static Surveying with an Operational GPS System, in *Proceedings of the Institute of Navigation GPS-93 Vol II*, Sixth International Technical Meeting of the Satellite Division of the Institute of Navigation, Salt Lake City, Utah, 1993.

Sovers, O.J. and Jacobs, C.S. Observation Model and Parameter Partials for the JPL VLBI Parameter Estimation Software "MODEST"-1994. *JPL Publication 83-39, Rev. 5.* NASA, USA, 1994.